Preparation of Well-Defined Dendrimer Encapsulated Ruthenium Nanoparticles and Their Evaluation in the Reduction of 4-Nitrophenol According to the Langmuir-Hinshelwood Approach

ARTICLE *in* LANGMUIR · OCTOBER 2013

Impact Factor: 4.46 · DOI: 10.1021/la402885k · Source: PubMed

Langmuir

Article

pubs.acs.org/Langmuir

Preparation of Well-Defined Dendrimer Encapsulated Ruthenium Nanoparticles and Their Evaluation in the Reduction of 4-Nitrophenol According to the Langmuir−Hinshelwood Approach

Nathan Charles Antonels and Reinout Meijboom*

Research Centre for Synthesis and Catalysis, Department of Chemistry, University of Johannesburg, P.O. Box 524, Auckland Park 2006, South Africa

Supporting Information

ABSTRACT: This study discusses the preparation of various sized dendrimer encapsulated ruthenium nanoparticles (RuDEN) with the use of the generation 4 (G4), generation 5 (G5), and generation 6 (G6) hydroxyl-terminated poly(amidoamine) (PAMAM-OH) dendrimers as templating agents. The size of the nanoparticles ranges from 1.1 to 2.2 nm. These catalysts were fully characterized using UV/vis spectrophotometry, infrared (IR) spectroscopy, and transmission electron microscopy (TEM). The RuDEN catalysts were evaluated in the reduction of 4-nitrophenol (4NP) in the presence of sodium borohydride (BH_4^-) for various concentrations of either. The kinetic data obtained were modeled to the Langmuir−Hinshelwood equation. The model allows the relation of the apparent rate constant to the total surface area S of the nanoparticle, the kinetic constant k which is related to the rate-determining step, and the adsorption constants K_{4NP} and K_{BH_4} for 4NP and borohydride, respectively. These parameters were calculated for each of the RuDENs, proving the Langmuir−Hinshelwood model to be suitable for the kinetic evaluation of RuDENs in the catalytic reduction of 4NP.

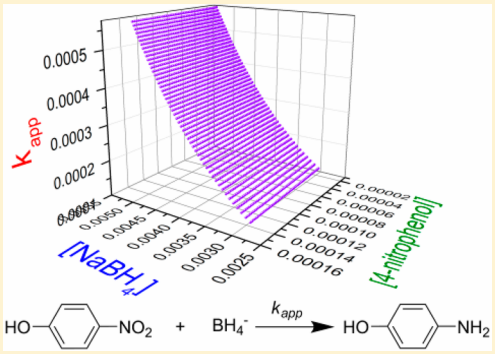

INTRODUCTION

The use of transition metal nanoparticles has gained widespread application in the field of catalysis.[1] Because of the high ratio of surface atoms to total atoms in transition metal nanoparticles, they closely approximate the behavior of conventional mononuclear transition metal catalysts. This property places transition metal nanoparticles on the border between homogeneous and heterogeneous catalysis, as they are able to operate as both.[2] Of great importance in the preparation of nanoparticles is the stabilization of metal nanoparticles and control of their size. The preparation of nanoparticles with a narrow size distribution is highly desirable. Aggregation of nanoparticles during synthesis results in the formation of thermodynamically favored larger sized nanoparticles, with a concomitant decrease in catalytic activity. There are various methods of stabilizing metal nanoparticles including the use of ionic liquids,[3] polymers,[4] low molecular weight[5] and macromolecular organic ligands,[6] to name a few. There are various modes of stabilization, including electrostatic stabilization and steric stabilization.[7] Electrostatic stabilization occurs when anions and cations associate with the nanoparticle surface, creating an electrical double layer with Coulombic repulsion preventing agglomeration. Steric stabilization occurs when large macromolecules associate with the nanoparticle surface. The stabilization and size of nanoparticles obtained are, however, dependent on the amount of these stabilizers, and a fine balance between amount of metal and stabilizer is needed.

The use of dendrimers as stabilizers allows for the templated preparation of nanoparticles in solution, and their stabilization is ensured by internal functional groups on the dendrimer that can coordinate to the nanoparticle surface with minimal passivation.[6,8,9] Dendrimers are discrete, well-defined hyperbranched macromolecular polymers where their size is denoted by their generation.[10] In the synthetic methodology for the dendrimer templated preparation of transition metal nanoparticles, the size of the nanoparticle is controlled by the overall loading capacity of the dendrimer for a particular transition metal complex and, more importantly, by the metal ion:dendrimer ratio. One of the most commonly used dendrimers in the preparation of transition metal nanoparticles are the commercially available poly(amidoamine) (PAMAM) dendrimers.[6] This class of dendrimers has tertiary amines present within its branches that provide sites for the coordination of transition metal complexes. Different sized nanoparticles can therefore be prepared by using different sized dendrimers where higher generation dendrimers are able to partition a larger amount of transition metal complexes into its interior.[6]

Ruthenium nanoparticles are known for their activity in hydrogenation reactions[11−15] and have been reviewed for

Received: July 27, 2013
Revised: September 27, 2013
Published: October 2, 2013

various catalytic systems, comprising ruthenium nanoparticles stabilized by polymers, alcohols, ionic ligands, various organic ligands, and solid supports.[16,17] Despite the progress in the preparation of dendrimer encapsulated transition metal nanoparticles, there are few articles cited for the preparation and utilization of monometallic dendrimer encapsulated ruthenium metal nanoparticles (RuDEN) and their evaluation as catalysts. One of the first preparations of ruthenium dendrimer encapsulated nanoparticles was conducted by Lafaye et al., who prepared ruthenium DENs and immobilized the nanoparticles on an alumina support.[18,19] Superior control of the nanoparticle size was achieved compared to Ru/Al_3O_3 prepared by wetness impregnation using an aqueous solution of $RuCl_3$. The preparation of these ruthenium DENs suffers from the lengthy 48−72 h period it takes for full coordination of the ruthenium to the tertiary amine—a procedure that was improved upon by Stevenson et al.[20] Their study utilized the partial galvanic displacement of nickel by ruthenium from a PAMAM−OH/Ni complex and then the subsequent reduction of this complex by sodium borohydride to yield bimetallic Ru/Ni DENs. Galvanic displacement reactions have been utilized by Crooks et al. and proves a facile method in the preparation of bimetallic dendrimer encapsulated nanoparticles.[21−23] In the case of the research conducted by Stevenson et al., they never mentioned this galvanic displacement used for the complete displacement of nickel to form monometallic RuDENs. The Ru/Ni DENs were briefly evaluated in the catalytic reduction of 4-nitrophenol (4NP) where the catalytic activity was enhanced by the presence of nickel when compared to monometallic RuDENs.[20]

The catalytic reduction of 4NP has been used as a benchmark reaction by many research groups for the evaluation of the catalytic activity of metal nanoparticles, owing to its ease of execution.[24−28] The reaction is conducted in aqueous media and can easily be followed using UV/vis spectrophotometry by observing the disappearance of the phenolate absorbance peak at λ 400 nm upon reduction of 4NP to 4-aminophenol (4AP). Despite the widespread use of this reaction, there have been relatively few investigations into the mechanism involved in this reaction.

Esumi et al. investigated the effect of various generations of PPI and PAMAM dendrimers used to prepare Pt, Pd, and Ag DENs on the rate of 4NP reduction and found the reaction to be diffusion controlled.[29] Saha et al. investigated the effects of varying the concentration of 4NP in the evaluation of the catalytic activity of their catalytic system.[25] The study provided a few key insights into the mechanism of the reaction as depicted in Figure 1.

They concluded that the mechanism relies on adsorption of the reactant on the surface, then diffusion of the 4NP and BH_4^- molecule to the active site to form a surface complex, reaction of the surface complex to form the product, and finally desorption of the product.[25] Zhang et al. further dealt with the mechanistic aspect of this surface reaction by evaluating silver nanoclusters deposited on TiO_2.[30] They surmised the initial adsorption of BH_4^- for transferral of a surface hydrogen and subsequent adsorption of 4NP to the surface to react and form 4AP. This would suggest a Langmuir−Hinshelwood mechanistic model that requires both substrate and reactant to adsorb on the catalyst surface before reaction occurs. Wunder et al. conducted a more comprehensive kinetic evaluation of their platinum and gold nanoparticles supported in polyelectrolyte brushes for the reduction of 4NP.[31] The authors investigated

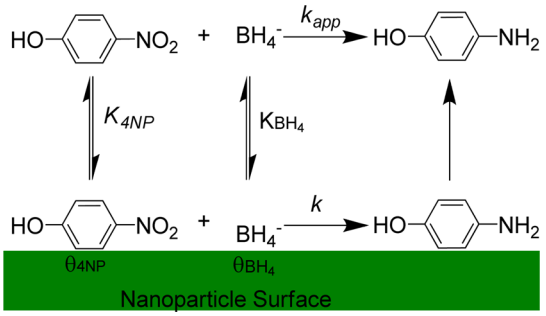

Figure 1. A simple mechanistic depiction of the 4NP reduction. The green shaded area represents the RuDEN surface where the reaction occurs. A BH_4^- and 4NP molecule adsorb on the catalyst surface in which case the adsorption and desorption of both are fast processes and can be modeled by the Langmuir−Hinshelwood mechanism and quantitatively described by the adsorption constants K_{BH_4} and K_{4NP}, respectively. The rate-determining step is the reduction of 4NP to 4AP and is described by the surface rate constant k.

both the effects of variation in 4NP concentration and BH_4^- concentration on the rate of the reaction. They confirmed that the catalytic reduction of 4NP in the presence of BH_4^- and metallic nanoparticles can be modeled according to Langmuir−Hinshelwood kinetics. Three constants were identified to describe the catalytic system: a kinetic constant, k, that describes the surface reactivity of the species and two thermodynamic adsorption constants, K_{4NP} for 4NP and K_{BH_4} for BH_4^-.

Given the aforementioned merits of ruthenium nanoparticle catalysts in hydrogenation reactions and the necessity for further insights into the kinetic mechanism of 4NP reduction, this study aims at providing a kinetic analysis of the RuDEN type catalysts in the evaluation of 4NP reduction with the use of the Langmuir−Hinshelwood mechanism. This mechanism requires the adsorption of both substrate and reactant to the nanoparticle surface with the rate-determining step being the reaction of the adsorbed species to form the product. The dendrimer structure does not provide a significant diffusion barrier as will be discussed later; therefore, the process is not expected to be diffusion controlled.

EXPERIMENTAL SECTION

Chemicals, Materials, and Instrumentation. The hydroxyl-terminated fourth- (G4OH), fifth- (G5OH), and sixth-generation (G6OH) poly(amidoamine) (PAMAM) dendrimers were purchased as methanol solutions (Sigma-Aldrich). The methanol was removed from these solutions prior to use under high vacuum at ambient temperature for 3 h. The $RuCl_3$ hydrate (99.98%), sodium borohydride, and 4-nitrophenol were purchased from Sigma-Aldrich and used as is. The sodium hydroxide was purchased from Associated Chemical Enterprises (ACE) and used as is. The Milli-Q (18 ΩM) deionized water was used in all experiments. The 4-nitrophenol reduction reactions were conducted in PLASTIBRAND PMMA standard disposable cuvettes purchased from Sigma-Aldrich.

UV/vis spectrophotometry spectra were obtained on a Shimadzu UV1800 UV/vis spectrophotometer. Fourier transform infrared (FTIR) spectra were obtained on a Bruker Tensor 27 FTIR spectrometer. Transmission electron microscopy (HRTEM) images were obtained on a JEOL JEM-2100F with an accelerating voltage of 200 kV equipped with a FEG source. HRTEM samples were prepared by a combination of drop deposition onto a holey carbon-covered TEM copper grid and wicking utilized to remove any excess sample. The average nanoparticle size was calculated by analyzing 250 nanoparticles from the obtained HRTEM images using ImageJ

dx.doi.org/10.1021/la402885k | Langmuir 2013, 29, 13433−13442

software.[32] The specific surface area was calculated from the average radius obtained and the total nanoparticle concentration based on the concentration of the dendrimer.

Preparation of RuDENs. The ruthenium DENs were synthesized according to the method previously described by Lafaye et al.,[18,19] and similarly, ruthenium DENs were synthesized by reacting hydroxyl-terminated G4-PAMAM-OH, G5-PAMAM-OH, and G6-PAMAM-OH with 40, 80, and 160 molar excesses of $RuCl_3 \cdot nH_2O$. Milli-Q water used was degassed for 30 min prior to use by bubbling with nitrogen. A 167 μL aliquot of 600 μM aqueous G4-PAMAM-OH (0.365 μmol) stock solution was transferred into a 50 cm^3 Schlenk tube. The reaction was diluted with 5475 μL of Milli-Q water added into the Schlenk tube while stirring. The solution was charged with an aqueous $RuCl_3$ (4 μmol) solution by pipetting 358 μL of a 11.18 mM $RuCl_3$ aqueous stock solution. This brings the total volume of the solution to 6 mL. The G4-PAMAM-OH/Ru mixture was stirred under nitrogen atmosphere for 72 h to allow complete complexation to occur. Thereafter, the ruthenium metallodendrimer was reduced by adding 4 × 1000 μL of freshly prepared 10 mM $NaBH_4$ (40 μmol) every 10 min over a 40 min period. The reaction was stirred under N_2 gas for 3 h to allow for complete reduction of ruthenium and formation of the RuDENs. Similarly, G5-RuDEN was prepared by reacting G5-PAMAM-OH (0.1 μmol) with aqueous $RuCl_3$ (8 μmol) and reducing with aqueous $NaBH_4$ (80 μmol) and in the case of G6-RuDEN reacting G6-PAMAM-OH (0.1 μmol) with aqueous $RuCl_3$ (16 μmol) and reducing with aqueous $NaBH_4$ (160 μmol) in a total volume of 10 mL. These give effective dendrimer concentrations of 10 μM.

Catalytic Reduction of 4NP Using RuDENs. The catalyst was prepared by transferring 2500 μL of the RuDEN (10 μM) solution to a N_2-purged round-bottom flask with degassed Milli-Q water (7500 μL), resulting in a 2.5 μM catalyst solution based on the dendrimer concentration. Each of the six cuvettes was charged with a set amount of the RuDEN catalyst solution that has a dendrimer encapsulated nanoparticle concentration of 2.5 μM. The required amount of $NaBH_4$ (0.1 or 0.2 M) solution is then pipetted into each cuvette followed by degassed Milli-Q water. The cuvettes were placed in the cuvette compartments of the UV/vis spectrophotometer, and the temperature was allowed to equilibrate at 298 K for 15 min. In the temperature-dependent studies, temperatures of 308, 318, and 328 K were used as well. The required amount of aqueous 4-nitrophenol (600 μM) solution was then pipetted into each cuvette to start the reduction reaction. The UV/vis spectrophotometer was programmed to record absorbance readings at λ 400 nm and λ 550 nm every few seconds. The catalytic reactions were conducted in triplicate to obtain the relevant kinetic data. Catalytic data were processed using Kinetic Studio software,[33] and all kinetic modeling was conducted using the Origin Pro 8.5 graphing and modeling software.[34]

RESULTS AND DISCUSSION

Preparation and Characterization of RuDENs. To obtain suitable DENs for use in the catalytic hydrogenation of 4NP, a synthetic method was adapted from Lafaye et al.[18] Prior to the evaluation of the ruthenium DENs the nanoparticles were characterized. UV/vis spectrophotometry was used to monitor the formation of the RuDENs as illustrated in Figure 2. Prior to reduction, the UV/vis spectrum displays an absorbance peak at λ 304 nm and λ 411 nm associated with the dendrimer−metal complex. This differs considerably from the peaks seen for $RuCl_3$ solution that displays absorbance peaks at λ 391 nm and λ 548 nm. Upon reduction, these two peaks disappear, the graph flattens out, and a new peak at λ 280 nm appears associated with the formation of RuDEN. The peak for RuDEN at λ 280 nm is consistent with that reported by Stevenson et al.[20] and most likely is associated with a Ru−amine type interaction occurring on the surface of the nanoparticle.[18] Similar characteristic absorbance peaks are seen for the remaining RuDEN catalysts that were prepared.

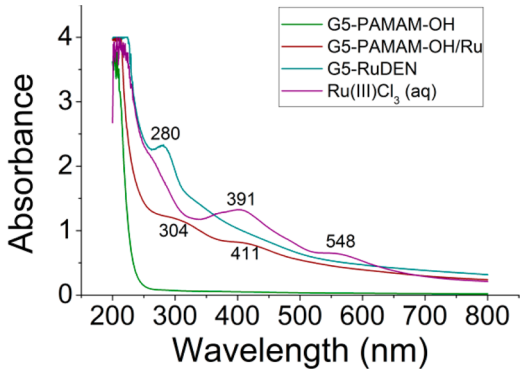

Figure 2. UV/vis spectra for the G5-PAMAM-OH dendrimer, G5-PAMAM-OH/Ru metallodendrimer, G5-RuDEN, and aqueous Ru(III)Cl_3.

Fourier transform infrared (FTIR) analysis was conducted on the dendrimer and dendrimer−metal complex prior to reduction, to further ascertain the coordination of ruthenium to the tertiary amines (see Supporting Information for tabulated data). In each case, the absorption bands for the vibrational stretches are within a similar range for each of the dendrimers. Absorption bands at ν 1064−1066 cm^{-1} and ν 1290−1294 cm^{-1} correspond to C−N stretching vibrations for the tertiary amine groups while absorption bands seen at ν 1550−1553 cm^{-1} correspond to the C−N stretching/C−N−H bending (amide II) vibrations.[35,36] The vibrational stretch observed at ν 1650−1652 cm^{-1} is assigned to the C═O stretching vibration (amide I).[37] Upon coordination of Ru(III) to the dendrimer, there is a significant shift in the absorption bands at ν 1290−1294 cm^{-1} to wavenumbers of 1260−1262 cm^{-1}, further confirming coordination of ruthenium to the dendrimer. The remaining stretching frequencies do not show such a significant change upon coordination.

HRTEM micrographs obtained for each of the RuDEN samples were analyzed to calculate the average particle diameter and a size distribution histogram of each of the samples generated as detailed in Figure 3. The average sizes of the nanoparticles for the various DENs were 1.2 ± 0.07, 1.4 ± 0.12, and 2.2 ± 0.26 nm for G4-RuDEN, G5-RuDEN, and G6-RuDEN, respectively. These values were used in the calculation of the specific surface area for each catalytic system. Because of the hydrophilic nature of PAMAM dendrimers, the DENs are ideally suited for conducting catalytic reactions in aqueous media. The polymeric nature of dendrimers allow for phenomena such as swelling of the macro-architecture to form an open solvated macro-environment for the catalytic reaction to occur. To ensure meaningful results, it is imperative that the total reactive surface area of the nanoparticles remains constant. Given the low concentration of RuDEN catalyst in each catalytic run and the additional stabilization provided by the dendritic architecture, Ostwald ripening is prevented and the total surface area unaffected.

The reduction of 4NP can be followed by monitoring changes in the absorbance peak at about λ 400 nm for the nitrophenolate anion upon reduction to 4AP (see Supporting Information for an illustration). The latter is accompanied by the growth in an absorbance peak at about λ 300 nm. The presence of isosbestic points proves that no side reactions occur, allowing for accuracy in interpretation of catalytic results.[38−40] Of importance is realizing the evolution of hydrogen gas during the reaction. This can cause shifts in the

dx.doi.org/10.1021/la402885k | Langmuir 2013, 29, 13433−13442

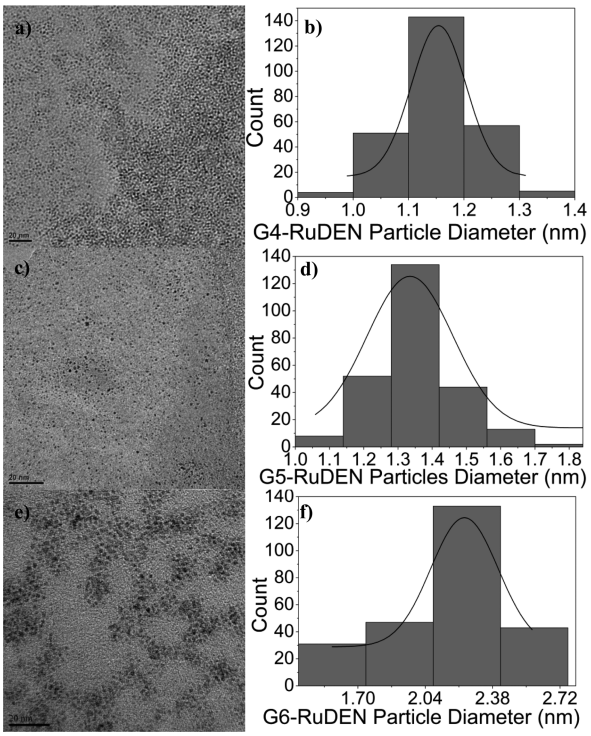

Figure 3. (a) HRTEM image of G4-RuDEN. (b) Histogram for the size distribution of G4-RuDEN. (c) HRTEM image of G5-RuDEN. (d) Histogram for the size distribution of G5-RuDEN. (e) HRTEM image of G6-RuDEN. (f) Histogram for the size distribution of G6-RuDEN.

entire spectrum and can be corrected by applying a baseline correction of the absorbance value at λ 400 nm with that of the absorbance at λ 550 nm. An induction period, classified as t_0, can be seen for catalytic runs during which no catalysis takes place and the reaction usually proceeds after this. In the case of the catalytic runs conducted in this study, the induction period is not always observed as the BH_4^- and catalyst interact during the 15 min period allowed for temperature equilibration prior to the addition of 4NP.

The kinetic analysis was conducted by collecting k_{app} data while keeping the BH_4^- constant and varying the 4NP concentration at the same temperature. A second set of measurements was conducted while keeping the 4NP concentration constant and varying the BH_4^- concentration. Two noteworthy observations are the usual increase in rate constant with increasing BH_4^- concentration and the decrease in k_{app} with increase in 4NP concentration as reported by Saha et al. and Wunder et al.[25,31] It makes sense that this reaction is not diffusion restricted as opposite behavioral trends would be observed, as was reported for the reduction of ferrocyanate(III) by borohydride with the use of gold nanoparticles as catalysts.[41]

One important factor in the kinetic studies is the consideration for possible diffusion barriers in the catalytic carrier. The RuDENs consist of a nanoparticle surface where the reaction occurs. Diffusion limitation occurs when the rate of catalytic turnover at the surface of the catalyst is considerably faster than the diffusion of the reactants. These two processes can be related to each other by use of the second Damköhler equation (DaII):

$$\mathrm{DaII} = \frac{k_{app} c^{n-1}}{\beta a} \quad (1)$$

Here k is the apparent rate constant, c is the concentration of the reactant, n is the order of the reaction, β is the mass transport coefficient, and a is the area of the interface which in this case is the volume normalized area of the nanoparticle. The β parameter is further defined as diffusion coefficient divided by the characteristic length scale, δ, a distance over which the mass transfer takes place. The diffusion coefficient previously calculated is 6.92×10^{-10} m^2/s.[42] The values for the remaining parameters of the three catalytic systems are detailed in Table 1.

Table 1. DaII Parameter Values for the RuDEN Catalysts Disqualifying Diffusion Limitations

catalyst	k_{app}[a] ($\times 10^{-6}$ s^{-1})	δ ($\times 10^{-9}$ m)	β (m s^{-1})	a (m^{-1})	DaII ($\times 10^{-6}$)
G4-RuDEN	3.96	4.5	0.154	501.76	5.13
G5-RuDEN	6.40	5.4	0.128	345.81	14.4
G6-RuDEN	2.90	6.7	0.103	437.20	6.42

[a] k at 0.1 mM 4NP and 5 mM $NaBH_4$.

In the evaluation of the DaII value, diffusion control is negligible since DaII $\ll$ 1. The three catalytic systems evaluated all give calculated DaII values of orders 10^{-5} or less. Given the low DaII value, the reduction of 4NP in the presence of the various PAMAM-OH carriers is not diffusion controlled.

Kinetic Analysis. *Investigation into the Effects of Surface Area Changes.* The rate of any reaction is directly proportional to the concentration of the catalyst available. In the case of homogeneous catalysts, catalytic activity is easily correlated with the total amount of catalyst present where each catalyst molecule represents a discrete active site. Heterogeneous nanoparticle catalysts requires that catalytic activity be correlated to the amount of potential active sites based on the total surface atoms in the particular batch of nanoparticle catalyst. This value may be calculated with some degree of certainty from the average diameter of the particle based on the assumption that the particle is spherical.

In the case of RuDENs, each dendrimer is likened to a discrete macromolecular container for a ruthenium nanoparticle. The nanoparticle concentration of any RuDEN solution in this study was therefore based on the concentration of the dendrimer for that particular solution and correlates with the total surface area of the DENs. The catalytic reactions were conducted under pseudo-first-order reaction conditions by ensuring a large excess of BH_4^-, relative to the amount of 4NP, present for each reaction. The apparent rate constant for the reduction of 4NP was calculated for the various DENs to quantitatively compare the catalytic activities. The rate constant is proportional to the total surface area as shown in eq 2:

$$-\frac{\mathrm{d}[4NP]}{\mathrm{d}t} = k_{app}[4\mathrm{NP}] = k_1 S[4\mathrm{NP}] \quad (2)$$

where [4NP] refers to the 4NP concentration at time t and k_1 is the apparent rate constant normalized to the surface area, S, of the Ru nanoparticle, which is normalized to the unit volume of the catalytic reaction system. The surface normalized rate constant was calculated by finding the slope of the plot k_{app}

dx.doi.org/10.1021/la402885k | Langmuir 2013, 29, 13433−13442

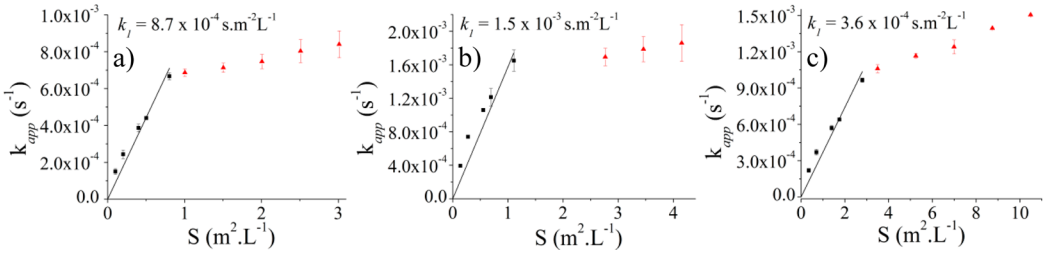

Figure 4. Apparent rate constant correlated with volume normalized surface area with the slope being the surface normalized rate constant k_1 and the red triangles indicating the volume normalized surface area where diffusion control occurs for (a) G4-RuDEN, (b) G5-RuDEN, and (c) G6-RuDEN.

against the volume normalized surface area S as given in the derived eq 3:

$$k_1 = \frac{k_{app}}{S} \tag{3}$$

Figure 4a–c illustrates the k_{app} values plotted against the surface area, S, for generations 4, 5, and 6 RuDENs at a constant 4NP and BH_4^- concentration, respectively. As previously mentioned, the BH_4^- concentration was kept in large excess of the 4NP concentration to ensure pseudo-first-order reaction conditions. The apparent rate constant shows a linear relationship with the surface area. This was expected since the reaction rate should increase with an increase in catalytic surface area. In each case, the surface normalized rate constant is the calculated slope of the line.

The surface area normalized rate constant k_1 was calculated for each of the RuDEN catalysts where G4-RuDEN, G5-RuDEN, and G6-RuDEN showed values of $(8.7 \pm 0.35) \times 10^{-4}$, $(1.5 \pm 0.08) \times 10^{-3}$, and $(3.6 \pm 0.16) \times 10^{-4}$ s m^{-2} L^{-1}, respectively. The red triangular data points correspond to the apparent rate constants where diffusion control occurs and therefore were not included in the calculation of the surface area normalized rate constant k_1. The surface normalized rate constants show an increase in value from G4-RuDEN to the G5-RuDEN and then a decrease going to G6-RuDEN from G5-RuDEN. The observed trend in surface rate constant values is possibly linked to the morphology as well the size of the nanoparticle surface for any given particle. One could argue that another possibility could be the difference in size of the dendrimer relative to the nanoparticle for each of the RuDEN catalysts and that a steric effect is in operation. The effect of dendrimer concentration on the rate constant was investigated by Esumi et al., who investigated the effect of the PAMAM dendrimer generation for the preparation of silver, platinum, and palladium nanoparticles and its evaluation in the catalytic reduction of 4NP.[29]

The effects of nanoparticle size on the catalytic rate of 4NP reduction have been studied by Lia et al., and an increase in reaction rate is realized for a decrease in nanoparticle size.[43] The amount of gold nanoparticles per catalytic reaction was kept constant, and the expected result was a correlation between the catalytic rate and the total surface area of the catalyst. The expectation is an increase in total surface area with an increase in the nanoparticle size, for a constant nanoparticle concentration, and hence increases in catalytic activity. The opposite trend was observed as the catalytic activity increased with a decrease in nanoparticle size despite the decrease in total surface area with decreasing nanoparticle size, a topic well discussed in reviews by Somorjai et al.[44,45] When considering the results obtained for the RuDENs in this study, the catalytic rate shows an increase for the smaller G4-RuDEN nanoparticles over that of the larger G6-RuDEN nanoparticles. It is important to remember that these are surface normalized rate constants, and they provide a first glance interpretation of the nanoparticle size effect.

In this case, the nanoparticle size effect is in agreement with that of the above-mentioned study reiterating that total surface area is not the only determining factor for catalytic activity when comparing nanoparticles of different sizes. The G5-RuDEN catalyst was of intermediate size for the three RuDEN catalysts. Contrary to the expected trend, there was not a decrease in the surface normalized rate constant going from G4-RuDEN to G5-RuDEN but a marked increase. The magnitude in size difference going from G4-RuDEN to G5-RuDEN is minimal compared to the size difference from G4-RuDEN to G6-RuDEN. The former are therefore in a more similar size regime when compared to G6-RuDEN.

Given this observation, the results suggest that G5-RuDENs are of an optimal size. To gain further insights into these systems, we evaluated the RuDEN catalysts with experimental design aimed at the eventual utilization of a Langmuir–Hinshelwood kinetic model.

Calculation of Langmuir–Hinshelwood Parameters. There are a few considerations that need to be taken into account before understanding the catalytic reduction of 4NP on the catalyst surface and analyzing the system using the Langmuir–Hinshelwood model.

In the case of the preparation of nanoparticles, sodium borohydride is an important reducing agent and serves as an electron source. The surface of metal nanoparticles become charged by injection of electrons from the borohydride ions to the nanoparticle surface,[41,46] a process that is observed by a shift in the surface plasmon band for the particular metal.[47,48] The presence of the plasmon band is, however, dependent on the size of the nanoparticle,[49] and the particles in this investigation are less than 3 nm in diameter associated with an absence of this plasmon band.[50] The process of borohydride ion adsorption on nanoparticle surfaces has been investigated. Studies show that adsorption of the borohydride ion on the metal nanoparticle surface is a fast and reversible process with rate-determining step in the hydrolysis being the cleavage of the OH bond in the water molecule.[51] Because both reactants adsorb to the nanoparticle surface for the reaction to occur, the interaction at the surface of the nanoparticle can be expressed in terms of Langmuir isotherms.

The kinetic data obtained for the reduction of 4NP using the various ruthenium DENs will be discussed in light of the Langmuir–Hinshelwood kinetic model. In the case of the borohydride adsorption, this is a fast and reversible process with a surface hydrogen being transferred to the nanoparticle surface upon adsorption. Subsequently, a 4NP molecule

dx.doi.org/10.1021/la402885k | *Langmuir* 2013, 29, 13433–13442

Table 2. Langmuir Freundlich Rate Constants and Adsorption Constants Obtained for RuDENs

catalyst	k [mol/(m^2 s)]	K_{4NP} [L/mol]	K_{BH_4} [L/mol]	n	m
G4-RuDEN	$(1.8 \pm 0.39) \times 10^{-5}$	90 ± 6	3.6 ± 1.1	0.37 ± 0.11	0.85 ± 0.08
G5-RuDEN	$(2.4 \pm 0.64) \times 10^{-5}$	87 ± 4	5.4 ± 1.1	0.56 ± 0.11	0.57 ± 0.15
G6-RuDEN	$(1.8 \pm 0.23) \times 10^{-5}$	94 ± 4	1.1 ± 0.1	0.54 ± 0.03	0.62 ± 0.05

adsorbs on the nanoparticle surface, and like the adsorption of borohydride, this process is fast and reversible. The rate-determining step is the reaction between the adsorbed 4NP molecule and surface hydrogen species to form 4AP. The 4AP then dissociates and the catalytic site can be further occupied by reactants. As a result, the rate of 4NP reduction is dependent on the nanoparticle surface coverage by 4NP and BH_4^- (eq 4):

$$\frac{d[4NP]}{dt} = -kS\theta_{4NP}\theta_{BH_4} \tag{4}$$

where k is the actual rate constant and θ_{4NP} and θ_{BH_4} are the surface coverage values on the nanoparticle surface for 4NP and BH_4^-, respectively. The surface coverage values are further defined by eqs 5 and 6:

$$\theta_{4NP} = \frac{(K_{4NP}[4NP])^n}{1 + (K_{4NP}[4NP])^n + (K_{BH_4}[BH_4])^m} \tag{5}$$

$$\theta_{BH_4} = \frac{(K_{BH_4}[BH_4])^m}{1 + (K_{4NP}[4NP])^n + (K_{BH_4}[BH_4])^m} \tag{6}$$

As discussed by Wunder et al.,[31] the kinetic data can be modeled on the Langmuir–Freundlich isotherm where the equation for k_{app}, derived from a substitution of eqs 4, 5, and 6 into eq 2, is

$$k_{app} = \frac{kSK_{4NP}^n[4NP]^{n-1}(K_{BH_4}[BH_4])^m}{(1 + (K_{4NP}[4NP]^{n-1})^n + (K_{BH_4}[BH_4])^m)^2} \tag{7}$$

where k is the actual rate constant (on the surface), S is the total surface area of the catalyst, K_{4NP} is the adsorption constant for 4NP on the catalysts surface, [4NP] is the concentration of the 4NP, K_{BH_4} is the adsorption constant of sodium borohydride on the catalyst surface, $[BH_4]$ is the concentration of BH_4^-, and n and m are Langmuir–Freundlich constants describing the heterogeneity of the catalyst surface.

The parameter boundary values were kept constant throughout each individual system to investigate whether the model would converge within the calculated apparent rate constant parameter boundaries. The parameter value boundaries are quite restricted and any changes cause a marked deviation of the experimental data from the model. Wunder et al. noted a similar observation for the kinetic evaluation of metal nanoparticles immobilized in polyelectrolyte brushes.[31] The calculated parameter values are listed in Table 2.

The parameter values give a quantitative explanation for the behavior of the apparent rate constants with the subsequent changes in concentrations of BH_4^- and 4NP. Figure 5 illustrates the fitting of the various catalytic data to the Langmuir–Hinshelwood equation (4). The increase in 4NP concentration caused a decrease in the apparent rate constant as the surface of the nanoparticle becomes saturated with 4NP molecules. This leads to a significant decrease in the reaction of BH_4^- with the surface of the nanoparticle and consequently a decrease in the rate of electron transfer to the nanoparticle surface. The

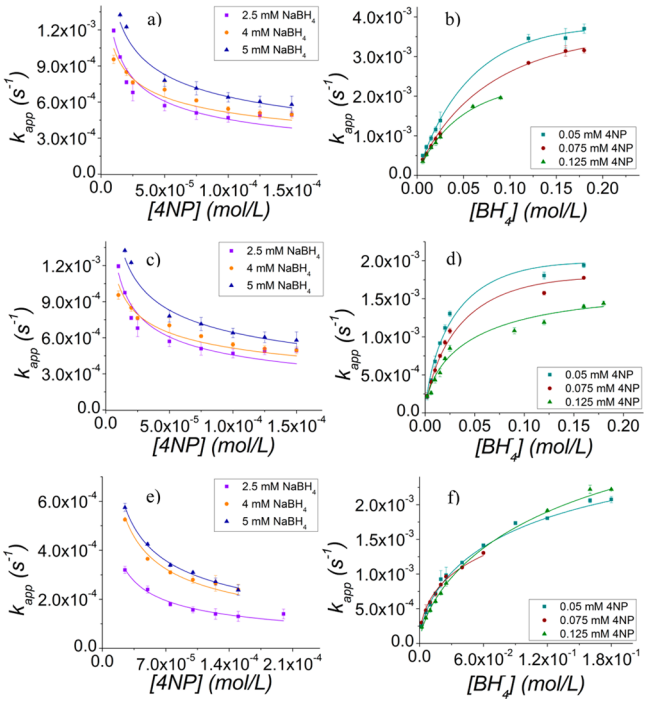

Figure 5. Parts a, c, and e detail the dependence of k_{app} on the changes in 4NP concentration according to the Langmuir–Hinshelwood mechanism for G4-RuDEN (surface area 0.5017 m^2 L^{-1}), G5-RuDEN (surface area 0.3458 m^2 L^{-1}), and G6-RuDEN (surface area 0.6994 m^2 L^{-1}), respectively. Parts b, d, and e detail the dependence of k_{app} on the changes in BH_4^- concentration according to the Langmuir–Hinshelwood mechanism for G4-RuDEN (surface area 0.5017 m^2 L^{-1}), G5-RuDEN (surface area 0.3458 m^2 L^{-1}), and G6-RuDEN (surface area 0.6994 m^2 L^{-1}), respectively. T = 298 K.

nonlinear behavior of the apparent rate constant values with increase in BH_4^- and 4NP concentration suggests competitive adsorption of substrate and reactant on the nanoparticle surface. An optimal concentration of both BH_4^- and 4NP exists where a maximum catalytic rate is observed.

The quality of the data was assessed by calculating plots of $k_{app}[4NP]$ versus $\theta_{4NP}\theta_{BH_4}$. This was derived from a simple rearrangement of the Langmuir–Hinshelwood equation (7) with substitution of the surface coverage values θ_{4NP} (5) and θ_{BH4} (6) to give eq 8a and subsequently the relation 8b.

$$k_{app}[4NP] = kS\theta_{4NP}\theta_{BH_4} \tag{8a}$$

$$kS = \frac{k_{app}[4NP]}{\theta_{4NP}\theta_{BH_4}} \tag{8b}$$

Figure 6a illustrates the data obtained for varying BH_4^- concentrations and Figure 6b the data obtained for varying 4NP concentrations. The slope of the straight line is the product of the kinetic constant, k, and the surface area, S, of the nanoparticle. These values are in agreement with the values calculated from k and S, considering the error associated with

dx.doi.org/10.1021/la402885k | Langmuir 2013, 29, 13433–13442

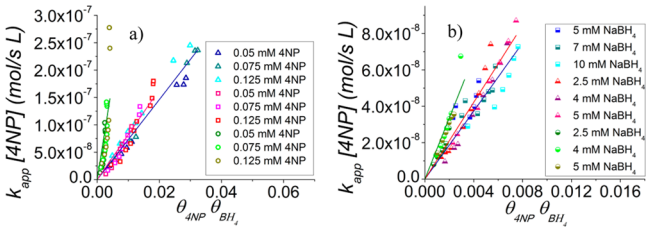

Figure 6. Plot of the product of apparent rate constant k_{app} and 4NP concentration [4NP] versus the product of the surface coverage for 4NP and BH_4^-, $\theta_{4NP}\theta_{BH_4}$. The solid line is the product of the rate constant k and surface area S. The squares, triangles, and circles represent G4-RuDEN (surface area 0.5017 m^2 L^{-1}), G5-RuDEN (surface area 0.3458 m^2 L^{-1}), and G6-RuDEN (surface area 0.6994 m^2 L^{-1}), respectively. (a) Illustration of the above-mentioned data for constant 4NP concentration. (b) Illustration of the above-mentioned data for constant BH_4^- concentration.

the calculation of both θ_{4NP} and θ_{BH_4}. Given the validity of the present fit, the Langmuir–Hinshelwood model sufficiently models the behavior of this catalytic reaction for RuDENs.

The results in Table 2 correlate with the findings for the surface normalized rate constants found earlier for the effects of surface area on the rate constant. Analyses of the adsorption constants help clarify the observed behavior. The kinetic constants, k, follow the same trend as the surface normalized rate constants, k_i, where the highest rate constant was realized for G5-RuDEN and the lowest for G6-RuDEN. The 4NP adsorption constants obtained for the different catalysts show minimal differences in values. When considering the values obtained for the BH_4^- adsorption constants, these are 25 times, 16 times, and 85 times larger than the 4NP adsorption constants for G4-RuDEN, G5-RuDEN, and G6-RuDEN, respectively.

An intermediate kinetic constant value was observed when evaluating G4-RuDEN. When comparing the nanoparticle size extremes for this set of catalysts, it is clear that there is an overall decrease in catalytic rate when only considering G4-RuDEN and G6-RuDEN. Given that this trend is not followed going from G4-RuDEN to G5-RuDEN, the results imply that G5-RuDEN represents an optimal sized nanoparticle for the catalytic reduction of 4NP. Nevertheless, the observed trend reflects through the parameters, K_{4NP} and K_{BH_4}, relative to each other where the increase in K_{BH_4} associated with a disproportional decrease in K_{4NP} displays a higher kinetic constant, k.

The model provided assumes all catalytic sites to be active. However, the calculation of heterogeneity exponents (Freundlich isotherms) related to the adsorption/desorption of 4NP and BH_4^- implies heterogeneity of the adsorption sites. This correlation of heterogeneity to studies in reaction kinetics at a nanoparticle surface was discussed by Zhou et al.[52] In this study, the heterogeneity was rationalized by a spontaneous and catalysis-induced surface restructuring. The heterogeneity values, n, for each of the catalysts are $n = 0.37$, $n = 0.56$, and $n = 0.54$ for G4-RuDEN, G5-RuDEN, and G6-RuDEN, respectively. This implies an increased heterogeneity from a perfectly Gaussian distribution of catalytically active sites defined by a n-value of one. The heterogeneity values for each system point to the surface not being uniform, but the difference in these values does not seem as significant for comparing the RuDEN catalytic systems, except when comparing G5-RuDEN and G6-RuDEN to G4-RuDEN where G4-RuDEN has a significantly lower n-value.

The increase in catalytic rate with decrease in size might be rationalized by the larger Fermi level shift when high electron injecting species are present such as the presence of BH_4^- ions in the 4NP reduction reaction.[53] This effect is certainly more pronounced for smaller nanoparticles such as those in the current study. The increase in catalytic rate with a decrease in nanoparticle size from G6-RuDEN to G4-RuDEN for this study agrees with similar trends observed for smaller nanoparticles with a higher fraction of low coordination sites than larger particles with a larger fraction of high-coordination surface sites.[54] Previous reports indicate that larger nanoparticles have a lower surface heterogeneity with surfaces terminated by large terraces of identical surface atoms. The increase in heterogeneity with decrease in nanoparticle size is met with a significant change in the statistical distribution of surface atom types[55] and concomitant increase in surface roughness.[56] A higher fraction of coordinatively unsaturated surface atoms therefore exists for smaller nanoparticles. This increase in surface roughness helps increase the chemisorption of both 4NP and BH_4^- where the effect is more evident in the latter when considering the K_{BH_4} values obtained.

Calculation of Thermodynamic Parameters. Table 3 presents the calculated thermodynamic data for each of the catalysts used in this study. The temperature-dependent studies were conducted for a 4NP and BH_4^- concentrations of 0.05 and 5 mM, respectively. Various groups have reported the activation energy for 4NP reduction albeit as catalyzed by different metals.[24,38,39,57,58] The activation energy was calculated for the apparent rate constant and therefore contains a dependency on the adsorption constants for BH_4^- and 4NP. To account for these adsorption constants, further experiments are required, but for the sake of comparison between the different RuDENs, this evaluation is sufficient. No literature precedence has been found to account for the thermodynamic parameter values of ruthenium nanoparticles in the evaluation of 4NP reduction in the presence of BH_4^-. The thermodynamic ΔH and ΔS parameters displayed in Table 3 will therefore be used mostly to discuss the nature of the reaction and the activation energy will be compared to literature values to ascertain whether RuDEN activation energies are within an expected range.

Table 3. Thermodynamic Parameters E_a, ΔH, and ΔS for the Various RuDEN Catalysts

catalyst	E_a (kJ/mol)	ΔH (kJ/mol)	ΔS (J/(mol K))
G4-RuDEN	16.45 ± 0.73	14.08 ± 0.61	−256.55 ± 1.82
G5-RuDEN	23.35 ± 0.11	13.72 ± 0.37	−262.76 ± 0.54
G6-RuDEN	28.74 ± 1.60	26.89 ± 1.86	−219.90 ± 5.28

The activation energies of various other nanoparticle systems evaluated in the reduction of 4NP are listed in Table 4. It is clear from the range of these values that the investigated system has activation energies well within the expected values when compared to obtained values for RuDENs depicted in Table 4. In the case of the activation energies observed for the RuDEN catalysts, there is a decrease in the activation energy with a decrease in the particle size. This correlates with the expected trend of increase in the rate of the reaction with decrease in the particle size as mentioned earlier and concomitant increase in surface roughness. In each case, the reaction is endothermic as

dx.doi.org/10.1021/la402885k | *Langmuir* 2013, 29, 13433−13442

Table 4. Activation Energy Values for Different Nanoparticle Catalyst Systems Evaluated in the Reduction of 4NP

nanoparticle catalyst	E_a (kJ/mol)	ref
silver	41	40
silver/calcium alginate	13.8	25
gold/calcium alginate	20.5	25
gold/polyelectrolyte brush	43	59
CTAB stabilized gold rods	38	28
Pt nanocubes	14	60
Pt nanocubes/polystyrene microspheres	12	60
citrate stabilized gold nanoparticles	21	27
partially hollow gold nanoboxes	55	24
hollow gold nanoboxes	44	24
gold nanocages	28	24

reflected in the positive ΔH values 14.08, 13.72, and 26.89 kJ mol^{-1} for G4-RuDEN, G5-RuDEN, and G6-RuDEN, respectively. The entropy values obtained for each of the catalyst evaluations are all negative which agree with the endothermic nature of the reaction and suggesting energy input needed for the reaction to continue.

CONCLUSION

In this study, we have demonstrated that the Langmuir–Hinshelwood model, which assumes the adsorption of both reactants of the surface of the catalyst, is applicable to the study of 4NP reduction by RuDENs in the presence of BH_4^-. The model allows for the calculation of three constants related to each system: the kinetic constant, k, that describes the surface reactivity of the adsorbed species and the two thermodynamic adsorption constants K_{4NP}, for 4NP, and K_{BH_4}, for BH_4^-. The correlation between size and catalytic rate was demonstrated where smaller nanoparticles display a higher catalytic rate. For the investigated catalysts there appears to be an optimum nanoparticle size for the catalytic reaction.

ASSOCIATED CONTENT

Supporting Information

FTIR tabulated data and UV/vis spectrophotometry scanning kinetics of nitrophenol reduction. This material is available free of charge via the Internet at http://pubs.acs.org.

AUTHOR INFORMATION

Corresponding Author

*E-mail rmeijboom@uj.ac.za (R.M.).

Notes

The authors declare no competing financial interest.

ACKNOWLEDGMENTS

This work is based on the research supported in part by the National Research Foundation of South Africa (Grant specific unique reference number (UID) 85386), The University of Johannesburg for funding, Shimadzu for the use of their donated equipment, and Tumisang, a research academy for undergraduates student that assisted with the project. I thank Stefanie Wunder from the Helmholtz Zentrum Berlin for her advice on the modeling of the 4NP reduction kinetic data.

REFERENCES

(1) Astruc, D. *Nanoparticles and Catalysis*; Wiley-VCH: Weinheim, 2008; pp 129–249.

(2) Astruc, D.; Lu, F.; Aranzaes, J. R. Nanoparticles as Recyclable Catalysts: The Frontier between Homogeneous and Heterogeneous Catalysis. *Angew. Chem., Int. Ed.* **2005**, *44*, 7852–7872.

(3) Migowski, P.; Dupont, J. Catalytic Applications of Metal Nanoparticles in Imidazolium Ionic Liquids. *Chem.—Eur. J.* **2007**, *13*, 32–39.

(4) *Nanoparticles: From Theory to Application*, 2nd Completely Revised and Updated Edition; Schmid, G., Ed.; Wiley-VCH: Weinheim, 2010; p 217.

(5) Mourdikoudis, S.; Liz-Marzán, L. M. Oleylamine in Nanoparticle Synthesis. *Chem. Mater.* **2013**, *25*, 1465–1476.

(6) Niu, Y.; Crooks, R. M. Dendrimer-Encapsulated Metal Nanoparticles and Their Applications to Catalysis. *C. R. Chim.* **2003**, *6*, 1049–1059.

(7) Pachón, L. D.; Rothenberg, G. Transition-Metal Nanoparticles: Synthesis, Stability and the Leaching Issue. *Appl. Organomet. Chem.* **2008**, *22*, 288–299.

(8) Myers, V. S.; Weir, M. G.; Carino, E. V.; Yancey, D. F.; Pande, S.; Crooks, R. M. Dendrimer-Encapsulated Nanoparticles: New Synthetic and Characterization Methods and Catalytic Applications. *Chem. Sci.* **2011**, *2*, 1632–1646.

(9) Crooks, R. M.; Zhao, M.; Sun, L.; Chechik, V.; Yeung, L. K. Dendrimer-Encapsulated Metal Nanoparticles: Synthesis, Characterization, and Applications to Catalysis. *Acc. Chem. Res.* **2001**, *34*, 181–190.

(10) Bosman, A. W.; Janssen, H. M.; Meijer, E. W. About Dendrimers: Structure, Physical Properties, and Applications. *Chem. Rev.* **1999**, *99*, 1665–1688.

(11) Huang, J.; Jiang, T.; Han, B.; Wu, W.; Liu, Z.; Xie, Z.; Zhang, J. A Novel Method to Immobilize Ru Nanoparticles on SBA-15 Firmly by Ionic Liquid and Hydrogenation of Arene. *Catal. Lett.* **2005**, *103*, 59–62.

(12) Silveira, E. T.; Umpierre, A. P.; Rossi, L. M.; Machado, G.; Morais, J.; Soares, G. V.; Baumvol, I. J. R.; Teixeira, S. R.; Fichtner, P. F. P.; Dupont, J. The Partial Hydrogenation of Benzene to Cyclohexene by Nanoscale Ruthenium Catalysts in Imidazolium Ionic Liquids. *Chem.—Eur. J.* **2004**, *10*, 3734–3740.

(13) Zahmakıran, M.; Tonbulz, Y.; Özkar, S. Ruthenium (0) Nanoclusters Supported on Hydroxyapatite: Highly Active, Reusable and Green Catalyst in the Hydrogenation of Aromatics under Mild Conditions with an Unprecedented Catalytic Lifetime. *Chem. Commun.* **2010**, *46*, 4788–4790.

(14) Rossi, L. M.; Machado, G. Ruthenium Nanoparticles Prepared from Ruthenium Dioxide Precursor: Highly Active Catalyst for Hydrogenation of Arenes under Mild Conditions. *J. Mol. Catal. A: Chem.* **2009**, *298*, 69–73.

(15) Ning, J.; Xu, J.; Liu, J.; Lu, F. Selective Hydrogenation of Benzene to Cyclohexene over Colloidal Ruthenium Catalyst Stabilized by Silica. *Catal. Lett.* **2006**, *109*, 175–180.

(16) Stolle, A.; Gallert, T.; Schmöger, C.; Ondruschka, B. Hydrogenation of Citral: a Wide-Spread Model Reaction for Selective Reduction of α,β-Unsaturated Aldehydes. *RSC Adv.* **2013**, *3*, 2112–2153.

(17) Lara, P.; Philippot, K.; Chaudret, B. Organometallic Ruthenium Nanoparticles: A Comparative Study of the Influence of the Stabilizer on Their Characteristics and Reactivity. *ChemCatChem* **2013**, *5*, 28–45.

(18) Lafaye, G.; Williams, C. T.; Amiridis, M. D. Synthesis and Microscopic Characterization of Dendrimer-Derived Ru/Al_2O_3 Catalysts. *Catal. Lett.* **2004**, *96*, 43–47.

(19) Lafaye, G.; Siani, A.; Mare, P.; Williams, C. T. Particle Size Control in Dendrimer-Derived Supported Ruthenium Catalysts. *J. Phys. Chem. B* **2006**, *110*, 7725–7731.

(20) Marvin, K. A.; Thadani, N. N.; Atkinson, C. A.; Keller, E. L.; Stevenson, K. J. Preparation and Catalytic Evaluation of Ruthenium-Nickel Dendrimer Encapsulated Nanoparticles via Intradendrimer Redox Displacement of Nickel Nanoparticles. *Chem. Commun.* **2012**, *48*, 6289–6291.

(21) Pande, S.; Weir, M. G.; Zaccheo, B. A.; Crooks, R. M. Synthesis, Characterization, and Electrocatalysis Using Pt and Pd Dendrimer-Encapsulated Nanoparticles Prepared by Galvanic Exchange. *New J. Chem.* **2011**, *35*, 2054−2060.
(22) Yancey, D. F.; Zhang, L.; Crooks, R. M.; Henkelman, G. Au@Pt Dendrimer Encapsulated Nanoparticles as Model Electrocatalysts for Comparison of Experiment and Theory. *Chem. Sci.* **2012**, *3*, 1033−1040.
(23) Iyyamperumal, R.; Zhang, L.; Henkelman, G.; Crooks, R. M. Efficient Electrocatalytic Oxidation of Formic Acid Using Au@Pt Dendrimer-Encapsulated Nanoparticles. *J. Am. Chem. Soc.* **2013**, *135*, 5521−5524.
(24) Zeng, J.; Zhang, Q.; Chen, J.; Xia, Y. A Comparison Study of the Catalytic Properties of Au-Based Nanocages, Nanoboxes, and Nanoparticles. *Nano Lett.* **2010**, *10*, 30−35.
(25) Saha, S.; Pal, A.; Kundu, S.; Basu, S.; Pal, T. Photochemical Green Synthesis of Calcium-Alginate-Stabilized Ag and Au Nanoparticles and Their Catalytic Application to 4-Nitrophenol Reduction. *Langmuir* **2010**, *26*, 2885−2893.
(26) Pradhan, N.; Pal, A.; Pal, T. Silver Nanoparticle Catalyzed Reduction of Aromatic Nitro Compounds. *Colloids Surf., A* **2002**, *196*, 247−257.
(27) Panigrahi, S.; Basu, S.; Praharaj, S.; Pande, S.; Jana, S.; Pal, A.; Gosh, S. K.; Pal, T. J. Synthesis and Size-Selective Catalysis by Supported Gold Nanoparticles: Study on Heterogeneous and Homogeneous Catalytic Process. *J. Phys. Chem. C* **2007**, *111*, 4596−4605.
(28) Khalavka, Y.; Becker, J.; Sönnichsen, C. Synthesis of Rod-Shaped Gold Nanorattles with Improved Plasmon Sensitivity and Catalytic Activity. *J. Am. Chem. Soc.* **2009**, *131*, 1871−1875.
(29) Esumi, K.; Isono, R.; Yoshimura, T. Preparation of PAMAM- and PPI-Metal (Silver, Platinum,and Palladium) Nanocomposites and Their CatalyticActivities for Reduction of 4-Nitrophenol. *Langmuir* **2004**, *20*, 237−243.
(30) Zhang, H.; Li, X.; Chen, G. Ionic Liquid-Facilitated Synthesis and Catalytic Activity of Highly Dispersed Ag Nanoclusters Supported on TiO_2. *J. Mater. Chem.* **2009**, *19*, 8223.
(31) Wunder, S.; Polzer, F.; Lu, Y.; Mei, Y.; Ballauff, M. Kinetic Analysis of Catalytic Reduction of 4-Nitrophenol by Metallic Nanoparticles Immobilized in Spherical Polyelectrolyte Brushes. *J. Phys. Chem. C* **2010**, *114*, 8814−8820.
(32) Rasband, W. ImageJ, 1.47v; National Institute of Health, 2013.
(33) Kinetic Studio, 2.0.8.14953; TGK Scientific Limited, 2010.
(34) OriginPro 8.5.0 SR1, OriginLab Corporation, One Roundhouse Plaza Northampton, 2010.
(35) Socrates, G. *Infrared and Raman Characteristic Group Frequencies: Tables and Charts*, 3rd ed.; Wiley: Chichester, 2001.
(36) Lin-Vien, D.; Colthup, N. B.; Fateley, W. G.; Grasselli, J. G. *Infrared and Raman Characteristic Frequencies of Organic Molecules*; Academic Press: New York, 1991.
(37) Ishida, K. P.; Griffths, P. R. Comparison of the Amide I/II Intensity Ratio of Solution and Solid-State Proteins Sampled by Transmission, Attenuated Total Reflectance, and Diffuse Reflectance Spectrometry. *Appl. Spectrosc.* **1993**, *47*, 584−589.
(38) Mei, Y.; Lu, Y.; Polzer, F.; Ballauff, M. Catalytic Activity of Palladium Nanoparticles Encapsulated in Spherical Polyelectrolyte Brushes and Core−Shell Microgels. *Chem. Mater.* **2007**, *19*, 1062−1069.
(39) Mei, Y.; Sharma, G.; Lu, Y.; Ballauff, M. High Catalytic Activity of Platinum Nanoparticles Immobilized on Spherical Polyelectrolyte Brushes. *Langmuir* **2005**, *21*, 12229−12234.
(40) Pradhan, N.; Pal, A.; Pal, T. Silver Nanoparticle Catalyzed Reduction of Aromatic Nitro Compounds. *Colloids Surf., A* **2002**, *196*, 247−257.
(41) Carregal-Romero, S.; Pérez-Juste, J.; Hervés, P.; Liz-Marzán, L. M.; Mulvaney, P. Colloidal Gold-Catalyzed Reduction of Ferrocyanate (III) by Borohydride Ions: A Model System for Redox Catalysis. *Langmuir* **2010**, *26*, 1271−1277.
(42) Bielejewska, A.; Bylina, A.; Duszczyk, K.; Fiałkowski, M.; Hołyst, R. Evaluation of Ligand-Selector Interaction from Effective Diffusion Coefficient. *Anal. Chem.* **2010**, *82*, 5463−5469.
(43) Kundu, S.; Wang, K.; Liang, H. Size-Selective Synthesis and Catalytic Application of Polyelectrolyte Encapsulated Gold Nanoparticles Using Microwave Irradiation. *J. Phys. Chem. C* **2009**, *113*, 5157−5163.
(44) Musselwhite, N.; Somorjai, G. A. Investigations of Structure Sensitivity in Heterogeneous Catalysis: From Single Crystals to Monodisperse Nanoparticles. *Top. Catal.* Aug 2013; DOI 10.1007/s11244-013-0150-y. Springerlink http://link.springer.com/article/10.1007/s11244-013-0150-y (accessed 22/09/13).
(45) An, K.; Somorjai, G. A. Size and Shape Control of Metal Nanoparticles for Reaction Selectivity in Catalysis. *ChemCatChem* **2012**, *4*, 1512−1524.
(46) Henglein, A.; Lilie, J. Storage of Electrons in Aqueous Solution: the Rates of Chemical Charging and Discharging the Colloidal Silver Microelectrode. *J. Am. Chem. Soc.* **1981**, *103*, 1059−1066.
(47) Ung, T.; Liz-Marzán, L. M.; Mulvaney, P. Redox Catalysis Using Ag@SiO_2 Colloids. *J. Phys. Chem. B* **1999**, *103*, 6770−6773.
(48) Sardar, R.; Funston, A. M.; Mulvaney, P.; Murray, R. W. Gold Nanoparticles: Past, Present, and Future. *Langmuir* **2009**, *25*, 13840−13851.
(49) Moores, A.; Goettmann, F. The Plasmon Band in Noble Metal Nanoparticles: an Introduction to Theory and Applications. *New J. Chem.* **2006**, *30*, 1121−1132.
(50) Scaiano, J. C.; Netto-Ferreira, J. C.; Alarcon, E.; Billone, P.; Alejo, C. J. B.; Crites, C.-O. L.; Decan, M.; Fasciani, C.; González-Béjar, M.; Hallett-Tapley, G.; Grenier, M.; McGilvray, K. L.; Pacioni, N. L.; Pardoe, A.; René-Boisneuf, L.; Schwartz-Narbonne, R.; Silvero, M. J.; Stamplecoskie, K. G.; Wee, T.-L. Tuning Plasmon Transitions and Their Applications in Organic Photochemistry. *Pure Appl. Chem.* **2011**, *83*, 913−930.
(51) Guella, G.; Patton, B.; Miotello, A. Kinetic Features of the Platinum Catalyzed Hydrolysis of Sodium Borohydride from ^{11}B NMR Measurements. *J. Phys. Chem. C* **2007**, *111*, 18744−18750.
(52) Zhou, X.; Xu, W.; Liu, G.; Panda, D.; Chen, P. Size-Dependent Catalytic Activity and Dynamics of Gold Nanoparticles at the Single-Molecule Level. *J. Am. Chem. Soc.* **2010**, *132*, 138−146.
(53) Henglein, A. Physicochemical Properties of Small Metal Particles in Solution: "Microelectrode" Reactions, Chemisorption, Composite Metal Particles, and the Atom-to-Metal Transition. *J. Phys. Chem.* **1993**, *97*, 5457−5471.
(54) Härle, H.; Metka, U.; Volpp, H.-R.; Wolfrum, J. Pressure Dependence (10^{-8}−1000 mbar) of the Vibrational Spectra of CO Chemisorbed on Polycrystalline Platinum Studied by Infrared−Visible Sum-Frequency Generation. *Phys. Chem. Chem. Phys.* **1999**, *1*, 5059−5064.
(55) Hardeveld, R. V.; Hartog, F. The Statistics of Surface Atoms and Surface Sites on Metal Crystals. *Surf. Sci.* **1969**, *15*, 189−230.
(56) Song, H.; Rioux, R. M.; Hoefelmeyer, J. D.; Komor, R.; Niesz, K.; Grass, M.; Yang, P.; Somorjai, G. A. Hydrothermal Growth of Mesoporous SBA-15 Silica in the Presence of PVP-Stabilized Pt Nanoparticles: Synthesis, Characterization, and Catalytic Properties. *J. Am. Chem. Soc.* **2006**, *128*, 3027−3037.
(57) Mahmoud, M. A.; Snyder, B.; El-Sayed, M. Polystyrene Microspheres: Inactive Supporting Material for Recycling and Recovering Colloidal Nanocatalysts in Solution. *J. Phys. Chem. Lett.* **2010**, *1*, 28−31.
(58) Lu, Y.; Mei, Y.; Walker, R.; Ballauff, M.; Dreschler, M. "Nanotree"-Type Spherical Polymer Brush Particles as Templates for Metallic Nanoparticles. *Polymer* **2006**, *47*, 4985−4995.
(59) Schrinner, M.; Polzer, F.; Mei, Y.; Lu, Y.; Haupt, B.; Ballauff, M.; Göldel, A.; Drechsler, M.; Preussner, J.; Glatzel, U. Mechanism of the Formation of Amorphous Gold Nanoparticles within Spherical Polyelectrolyte Brushes. *Macromol. Chem. Phys.* **2007**, *208*, 1542−1547.
(60) Mahmoud, M. A.; Snyder, B.; El-sayed, M. Polystyrene Microspheres: Inactive Supporting Material for Recycling and

Recovering Colloidal Nanocatalysts in Solution. *J. Phys. Chem. Lett.* **2010**, *1*, 28−31.